Confluentes Math.
1, 0 (-1) 000-000

EXISTENCE ET STABILITÉ DE SOLUTIONS NON CARACTÉRISTIQUES ET STATIONNAIRES DES ÉQUATIONS DE NAVIER-STOKES NON ISENTROPIQUES SUR UN INTERVALLE

BLAKE BARKER, BENJAMIN MELINAND, AND KEVIN ZUMBRUN

Abstract. Nous étudions le problème du tube de choc, établissant l'existence et la stabilité de solutions stationnaires des équations de Navier-Stokes non isentropiques pour des données non caractéristiques. Nous présentons aussi des simulations numériques indiquant l'unicité et la stabilité de telles solutions. Dans le même temps, nous donnons un exemple d'équation d'état artificielle possédant une entropie convexe où l'unicité n'a pas lieu. Ce phénomène est associé à une instabilité et une bifurcation de Hopf de solutions périodiques en temps.

Résumé. (*Existence and stability of steady noncharacteristic solutions on a finite interval of full compressible Navier–Stokes equations*) We treat the 1D shock tube problem, establishing existence of steady solutions of full (nonisentropic) polytropic gas dynamics with arbitrary noncharacteristic data. We present also numerical experiments indicating uniqueness and time-asymptotic stability of such solutions. At the same time, we give an example of an (artificial) equation of state possessing a convex entropy for which there holds nonuniqueness of solutions. This is associated with instability and Hopf bifurcation to time-periodic solutions.

Introduction

In this paper, continuing investigation in [32] of the isentropic case, we study by a combination of analytical and numerical techniques the existence, uniqueness, and stability of steady solutions of the full (nonisentropic) 1D compressible Navier–Stokes equations on a bounded interval, with noncharacteristic inflow-outflow boundary conditions, and more generally of hyperbolic-parabolic systems of conservation laws of similar abstract type.

This corresponds to the 1D version of the "shock tube" problem of describing flow in a finite length and width channel, with prescribed boundary conditions at the left and right ends. Our main interest is in *large-amplitude* data. Small-amplitude 1D existence, uniqueness, and spectral stability are shown for general symmetrizable systems in [33].

As developed in the viscous shock case [10, 7, 8, 23, 24], a convenient method to study spectral stability is via numerical Evans function investigations. A useful necessary condition, also based on Evans function considerations, is positivity of the stability index, a mod two count of the Morse index of the linearized operator about the wave. This was trivially evaluable in the isentropic case [32], but is complicated in general. In particular, it does not seem to be analytically evaluable for the nonisentropic case considered here.

We carry out here both full Evans function and stability index calculations at the same time, both using the numerical code STABLAB [9].

Keywords: Steady solutions, gas dynamics, Evans function.

0.1. **Description of main results.** Our main analytical result is the global existence of steady solutions of the full polytropic gas equations (1.1) (Theorem 3.7), proved by a Brouwer degree argument using detailed and special ODE estimates, applied to the "Cauchy-to-boundary value" map Ψ defined in Section 1.2. We show, moreover, that global uniqueness of solutions of (1.1) is roughly equivalent to transversality of steady profiles as solutions of the ODE connection problem (1.5)-(1.9). This is equivalent to the nonvanishing of the Jacobian $\det(d\Psi)$ of (1.9) (Proposition 4.1).

Nonvanishing of $\det(d\Psi)$ is also seen to be equivalent to nonvanishing of the stability index (Lemma 5.1). Hence a change in sign implies appearance of both nonuniqueness and instability: the usual "exchange of stability" scenario familiar from finite-dimensional ODE. Thus we may study uniqueness in passing, in the course of a larger study of spectral stability.

Augmenting our analytical results for the full polytropic gas equations, we carry out such a study in Section 6 by a systematic numerical Evans function investigation of the "feasible set" $\mathcal{C}_{u_0,e_0}$ of profiles realizable by numerical shootings. Our numerical findings are that, on the feasible set $\mathcal{C}_{u_0,e_0}$, the stability index is uniformly positive, indicating *uniqueness of large-amplitude solutions*, and that steady solutions exhibit *uniform spectral stability*. We note that nonlinear stability can be shown to follow from spectral stability by similar considerations to those of [32, Section 6]; see [33].

On the other hand, we show numerically in Section 7.1 that both uniqueness and stability can fail for gas dynamics with an artificial convex equation of state.

0.2. **Discussion and open problems.** The first local existence/uniqueness result for small-amplitude data was established in [28], in multi-D. We extend that result here to large-amplitude data in the 1-D case by a combination of analytical (existence) and numerical (uniqueness) investigation, establishing (numerically) time-evolutionary stability as well.

Our findings of global existence and uniqueness for the noncharacteristic problem parallel those of Lions [30] in the characteristic case $u = 0$ on the boundary, for which he shows global existence and uniqueness of solutions for arbitrary prescribed average density, in 1- and multi-D. However, they are obtained by quite different techniques, which, moreover, are special to 1D. Indeed, though perhaps intuitively expectable, especially given the uniform shock stability results of [23, 24] for the compressible Navier–Stokes equations, our results of large-amplitude existence, uniqueness and stability are obtained by a combination of exhaustive numerical investigations, and rather delicate degree-theoretic arguments specific to the equations of 1D polytropic gas dynamics under study.

Our investigations of stability belong, rather, to a newer family of investigations blending numerical and analytical techniques to study dynamics and bifurcation of shock waves and related solutions of hyperbolic-parabolic conservation and balance laws, cf. [23, 3, 5, 13, 37, 41].

In [37, 41] the case of steady solutions on a half-line was investigated and it was shown that instability of steady solutions can occur, even for the most standard ideal polytropic gas law. This suggests that the question of stability at least is not a foregone conclusion for steady solutions on the interval. Moreover, the nature of instablity found in [37, 41] involved change of sign in the stability index, which

in the present case would signal nonuniqueness as well. On the other hand, our numerical findings (Section 6) indicate that neither of these phenomena in fact occur for polytropic gas dynamics on the interval.

This begs the question whether such detailed and special arguments are necessary, or whether there might instead exist some more straightforward argument for all or part of our results via general principles, such as, e.g., existence of convex entropy as used in Section 3. We give a partial answer to this question in Section 7, exhibiting a counterexample involving an equation of state presented in [3] for which the equations of compressible gas dynamics possess a convex entropy, but global stability and uniqueness are violated. It is seen that the associated transition to instability can involve either steady bifurcation to multiple solutions, or *Hopf bifurcation to time-periodic solutions*. The latter phenomenon is significant as the first example of Hopf bifurcation for stationary solutions of compressible gas dynamics, similar to "galloping" or "cellular" instabilities in detonation [39].

It is an interesting question whether our existence result extends to general equations of state considered in [3]. Note that we obtain nonuniqueness results for a particular equation of states in Section 7. A further very interesting open problem is the extension of our large-amplitude existence results to the true multi-D shock tube problem, generalizing the small-amplitude existence-uniqueness results of [28], and the determination of stability of steady multi-D solutions even in the small-amplitude case.

1. Preliminaries

1.1. **Equations of motion.** The 1D compressible Navier–Stokes equations in Eulerian coordinates are

$$\begin{aligned} \rho_t + (\rho u)_x &= 0\,, \\ (\rho u)_t + (\rho u^2 + p)_x &= \alpha u_{xx}\,, \\ (\rho E)_t + (\rho u E + p u)_x &= \kappa T_{xx} + (\alpha u u_x)_x \end{aligned} \tag{1.1}$$

where

$$E = e + \frac{u^2}{2}, \quad p = \Gamma \rho e, \quad e = c_v T\,,$$

and $\nu = \frac{\kappa}{c_v}$. Here Γ, c_v, ν and α are fixed positive constants; see [15, 23, 24].

As described in [32] in the isentropic case, we seek steady solutions on the interval $[0, 1]$, with noncharacteristic inflow-outflow boundary conditions

$$(\rho, u, e)(0) = (\rho_0, u_0, e_0), \quad (u, e)(1) = (u_1, e_1). \tag{1.2}$$

By changing ρ by $\rho_0\rho$, u by $\frac{1}{\rho_0}u$, t by $\rho_0 t$ and e by $\frac{1}{\rho_0^2}e$ (notice that we can not change x without changing the length of the interval), we assume in the following that

$$\rho_0 = 1, \quad u_0, e_0, u_1, e_1 > 0. \tag{1.3}$$

1.2. **Profile equations and formulation as mapping problem.** Our main interest is the study of steady solutions, i.e. solutions of

$$\begin{aligned}(\rho u)_x &= 0\,,\\ (\rho u^2 + \Gamma\rho e)_x &= \alpha u_{xx},\\ \left(\rho u\left(e+\frac{u^2}{2}\right)+\Gamma\rho e u\right)_x &= \nu e_{xx} + (\alpha u u_x)_x\end{aligned} \tag{1.4}$$

together with (1.2). In order to find these steady solutions, we use a shooting method. Integrating (1.4) from 0 to x and rearranging using (1.3), there exists constants of integration $c = (c_1, c_2)$ to be determined so that we obtain similarly as in [24] the profile ODE

$$\begin{aligned}\frac{\alpha}{u_0}u' &= c_1 + u + \Gamma\frac{e}{u},\\ \frac{\nu}{u_0}e' &= c_2 - c_1 u - \frac{1}{2}u^2 + e,\end{aligned} \tag{1.5}$$

together with $\rho = \frac{u_0}{u}$ and with the initial data

$$\begin{aligned}u(0) &= u_0 > 0,\\ e(0) &= e_0 > 0.\end{aligned} \tag{1.6}$$

In this setting

$$c_1 = \frac{\alpha}{u_0}u'(0) - u_0 - \Gamma\frac{e_0}{u_0}\ ,\ c_2 = \frac{\nu}{u_0}e'(0) + \alpha u'(0) - e_0 - \frac{1}{2}u_0^2 - \Gamma e_0, \tag{1.7}$$

where u_0 and e_0 are given and $(u'(0), e'(0))$ has to be determined in order to satisfies $(u(1), e(1)) = (u_1, e_1)$.

The domain of the ODE is the set

$$\left\{(u,e) \in \mathbb{R}^2\ ,\ u > 0\right\}$$

for which the right hand side of (1.5) is well-defined and from which we can reconstruct ρ. Indeed, we remark that $u > 0$ is imposed by $\rho u =$ constant and $\rho > 0$. Hence we may ignore the variable ρ in the following. Note also that the physical solutions are the ones for which e is also positive.

For a fixed choice of left data (ρ_0, u_0, e_0) (meaning, by our previous normalization, just a fixed choice of u_0 and e_0), we define now the "Cauchy-to-boundary value" mapping

$$\Psi : (c_1, c_2) \to (u, e)(1), \tag{1.8}$$

where (u, e) denotes the maximal solution of (1.5)-(1.6) for the given value of $c = (c_1, c_2)$. Evidently, solutions of (1.2)-(1.4) thus correspond to solutions of the mapping problem

$$\Psi(c) = (u_1, e_1). \tag{1.9}$$

2. The feasible set

In (1.8), we did not specify the domain of c. It is indeed our first order of business to determine it. For a fixed choice of left data (u_0, e_0), we define the feasible set $\mathcal{C}_{u_0,e_0}$ as the set of all c for which (1.5)-(1.6) has a continuous solution (u, e) on $[0, 1]$ where u and e are both positive on $[0, 1]$. Note that $\mathcal{C}_{u_0,e_0}$ is not empty since

$(-u_0 - \Gamma\frac{e_0}{u_0}, -(1+\Gamma)e_0 - \frac{1}{2}u_0^2) \in \mathcal{C}_{u_0,e_0}$ (that corresponds to the constant solution of problem (1.5)-(1.6)). Then, we have the following crucial observation.

PROPOSITION 2.1. — *The set $\mathcal{C}_{u_0,e_0}$ is open and its boundary consists of c for which there exists continuous functions (u,e) on $[0,1]$, solution of Problem (1.5)-(1.6) on $[0,1)$, with u,e both positive on $[0,1)$ and such that $e(1)=0$.*

Before proving Proposition 2.1, we establish a preliminary result.

LEMMA 2.2. — *Let $c=(c_1,c_2)\in\mathbb{R}^2$. Let $x_*\in(0,1]$ such that a solution (u,e) of (1.5)-(1.6) is defined on $[0,x_*)$. We have the following statements :*

(i) If $e>0$ on $[0,x_*)$, then (u,e) is bounded on $[0,x_*)$ uniformly with respect to x_* and one can extend continuously (u,e) to x_*.

(ii) If there exists a constant $\tilde{e}>0$, $e\geqslant\tilde{e}>0$ on $[0,x_*)$, then there exists a constant $\tilde{u}>0$, $u\geqslant\tilde{u}$ on $[0,x_*)$.

(iii) If $(u,e)\to 0$ simultaneously as $x\to x_*$ with (u,e) both positive on $[0,x_*)$, then $c_1<0$ and $c_2<0$.

(iv) Assume $c_1<0$, $c_2<0$, (u,e) is a solution of (1.5)-(1.6) on $[0,x_*]$ and $u,e>0$ on $[0,x_*]$. For any $\varepsilon>0$, there exists $\delta>0$ depending only on c_1,c_2,ε such that if $u(x_*),e(x_*)\leqslant\delta$, there exists $\tilde{x}\in[x_*,x_*+\varepsilon]$ such that (u,e) extends continuously as a solution of (1.5)-(1.6) on $[0,\tilde{x})$ with $u,e>0$ on $[0,\tilde{x})$ and $e(x)\to 0$ as $x\to\tilde{x}$.

Remark 2.3. — As we will see in the proof of (iv), one can prove that if $c_1<0$, $c_2<0$ and (u,e) is a solution of (1.5)-(1.6) on $[0,1)$ with u and e both positive on $[0,1)$, there exists a constant $M>0$ depending only on c_1,c_2,Γ, such that for any $\delta>0$ small enough, for any $x_*\in(0,1)$, if $0<u(x_*),e(x_*)\leqslant\delta$, then $0<e\leqslant\delta$ and $0<u\leqslant M\delta$ on $[x_*,1)$.

Proof of Lemma 2.2. — (i) Since $e>0$ on $[0,x_*)$, we get

$$\begin{aligned}\frac{1}{2}\left(\frac{\alpha}{u_0}u^2+\frac{\nu}{u_0}e^2\right)' &= c_1u+u^2+\Gamma e+c_2e-c_1eu-eu^2/2+e^2\\ &\leqslant c_1u+u^2+\Gamma e+c_2e-c_1eu+e^2\\ &\leqslant \frac{1}{2}\left(c_1^2+u^2+2u^2+\Gamma^2+e^2+c_2^2+e^2+c_1^2e^2+u^2+e^2\right)\\ &\leqslant A\left(\frac{\alpha}{u_0}u^2+\frac{\nu}{u_0}e^2\right)+B\end{aligned}$$

for some constants $A,B>0$ depending only on c_1, c_2, Γ, α, ν, u_0. Hence, $|(u,e)|$ grows at most exponentially, in particular remaining bounded on $[0,x_*)$. Furthermore, u and e can be continuously extended to x_* since $(u^2)'$ and $(e^2)'$ are bounded and then integrable on $[0,x_*)$.

(ii) The term $\Gamma\frac{e}{u}$ in the u-equation serves as a barrier meaning that there exists $u_*>0$ such that for any $u\in(0,u_*]$, $c_1+u+\Gamma\frac{\tilde{e}}{u}\geqslant 0$.

(iii) Evidently, $c_1<0$, or else $u'>0$ for u, $e>0$, contradicting the assumed convergence to 0. Then, for $u>0$ sufficiently small, this implies that $-c_1u-\frac{1}{2}u^2>0$ and hence $\frac{\nu}{u_0}e'>c_2+e$. Therefore, $c_2<0$ or else $e'>0$ for $e>0$ and $u>0$ sufficiently small, again contradicting convergence. This proves (iii).

(iv) We assume now that c_1, $c_2<0$, that (u,e) are both positive on $[0,x_*]$ and that $u(x_*),e(x_*)\leqslant\delta$. By point (i), one can extend (u,e) as a solution of (1.5)-(1.6)

on a interval that strictly contains $[0, x_*]$. We introduce

$\tilde{x} = \sup\{x \leqslant x_* + \varepsilon \text{ , } (u, e) \text{ extends as a solution of (1.5)-(1.6) and are positive on } [0, x)\}$

and we keep the notation (u, e) for the solution on $[0, \tilde{x})$. We first note that so long as u and e remain less than $\frac{c_2}{c_1 - 1}$ on $[x_*, \tilde{x})$ we have $\frac{\nu}{u_0} e' < -\frac{1}{2}u^2 \leqslant 0$ and thus e is decreasing on $[x_*, \tilde{x})$. Next, based on the u-equation, several situations can happen around $x \in [x_*, \tilde{x})$:

(a) If $u(x) > \frac{-c_1 - \sqrt{c_1^2 - 4\Gamma e(x)}}{2}$, $u'(x) < 0$ and u is decreasing around x.

(b) If $u(x) = \frac{-c_1 - \sqrt{c_1^2 - 4\Gamma e(x)}}{2}$, $u'(x) = 0$, $u''(x) = \Gamma \frac{e'(x)}{u(x)} < 0$, u is decreasing around x.

(c) If $u(x) < \frac{-c_1 - \sqrt{c_1^2 - 4\Gamma e(x)}}{2}$, then $u < \frac{-c_1 - \sqrt{c_1^2 - 4\Gamma e}}{2} \leqslant 2\Gamma \frac{|e|}{|c_1|}$ around x.

Therefore, for δ small enough, $u \leqslant \max\left(1, \frac{2\Gamma}{|c_1|}\right)\delta$ and $\frac{\nu}{u_0} e' < \frac{c_2}{2}$ on $[x_*, \tilde{x})$ and e goes to zero as $x \to \tilde{x}$ with $|\tilde{x} - x_*| \leqslant \frac{2\nu}{u_0 |c_2|}\delta$. This proves assertion (iv). □

Thanks to this lemma we can assert that

$\mathcal{C}_{u_0, e_0} = \left\{c \in \mathbb{R}^2 \text{ , where } e > 0 \text{ on } [0, 1] \text{ , } (u, e) \text{ the maximal solution of (1.5)-(1.6)}\right\}.$

Proof of Proposition 2.1. — For $c = (c_1, c_2)$, we denote by (u, e) the maximal solution of Problem (1.5)-(1.6). Note that the following map is locally Lipschitz

$$\Phi : (u, e) \in \left\{(u, e) \in \mathbb{R}^2 \text{ , } u > 0\right\} \mapsto \left(c_1 + u + \frac{\Gamma e}{u} \text{ , } c_2 - c_1 u - \frac{1}{2}u^2 + e\right). \quad (2.1)$$

If $c \in \mathcal{C}_{u_0, e_0}$, then u and e are defined and positive on $[0, 1]$ and by continuous dependence on parameters of solutions of an ODE, c lies in the interior of $\mathcal{C}_{u_0, e_0}$. In particular $\mathcal{C}_{u_0, e_0}$ is open.

We assume in the following that $c \in \mathcal{C}^c_{u_0, e_0}$. Thanks to Lemma 2.2(i)-(ii), there exists $x_* \in (0, 1]$ such that u and e are defined and continuous on $[0, x_*)$, $u, e > 0$ on $[0, x_*)$ and (u, e) can be extended to x_* with $e(x_*) = 0$ and $u(x_*) \geqslant 0$. Note that x_* is the smallest point on $[0, 1]$ such that $e(x_*) = 0$ and $u(x_*) \geqslant 0$ and not necessary the right boundary of the domain of definition of (u, e). Our goal is to show that $c \in \partial\mathcal{C}_{u_0, e_0}$ if and only if $x_* = 1$. Three different situations can then occur.

Case (i) : $x_* = 1$ and then $e(1) = 0$.

Case (ii) : $u(x_*) > 0$ and $x_* < 1$. Then (u, e) is defined on an interval that strictly contains $[0, x_*]$ and $e'(x_*) \leqslant 0$. In that case let us show that e must actually cross 0 and must become negative as x crosses x_*. Since $u(x_*) > 0$, (u, e) is defined on an interval that strictly contains $[0, x_*]$ and $e'(x_*) \leqslant 0$. Several subcases occur.

Subcase (ii)(a) : If $e'(x_*) < 0$, e crosses 0 and becomes negative as x crosses x_*.

Subcase (ii)(b) : If $e'(x_*) = 0$ and $u(x_*) \neq -c_1$, then

$$\frac{\nu}{u_0} e''(x_*) = -(c_1 + u(x_*))u'(x_*) = -\frac{u_0}{\alpha}(c_1 + u(x_*))^2 < 0$$

and e crosses 0 and becomes negative as x crosses x_*.

Subcase (ii)(c) : If $e'(x_*) = 0$ and $u(x_*) = -c_1$, repeated differentiation shows that derivatives of e and u at x_* vanish to all orders. By analyticity of solutions of an analytic ODE (note that $u > 0$), $e \equiv 0$ and $u \equiv -c_1$, contradicting $e(0) = e_0 > 0$ so that this subcase can not occur.

With such a fact in hand, there exists $\varepsilon > 0$ small enough such that (u, e) is defined

on $[0, x_* + \varepsilon]$, e negative on $]x_*, x_* + \varepsilon]$ and u positive on $[0, x_* + \varepsilon]$. By continuous dependence on parameters that c lies in the interior of $\mathcal{C}^c_{u_0,e_0}$ and $c \notin \partial\mathcal{C}_{u_0,e_0}$.
Case (iii) : $u(x_*) = 0$ and $x_* < 1$. In this case, Lemma 2.2(iii) shows that c_1, $c_2 < 0$. Let $(\tilde{c}_1, \tilde{c}_2)$ close enough to (c_1, c_2) and denote by $(\tilde{u}, \tilde{e})$ the maximal solution of Problem (1.5)-(1.6) associated to $(\tilde{c}_1, \tilde{c}_2)$. We then take a δ associated to $\varepsilon = 1 - x_*$ in Lemma 2.2(iv) that works for any $(\tilde{c}_1, \tilde{c}_2)$ close enough to (c_1, c_2). By continuity of u and e, there exists a number $\mu > 0$ small enough such that $0 < u(x_* - \mu), e(x_* - \mu) \leqslant \frac{\delta}{2}$. Then, by continuous dependence on parameters, for any $(\tilde{c}_1, \tilde{c}_2)$ close enough to (c_1, c_2), $(\tilde{u}, \tilde{e})$ is defined on $[0, x_* - \mu]$ and $0 < \tilde{u}(x_* - \mu), \tilde{e}(x_* - \mu) \leqslant \delta$. Lemma 2.2(iv) shows that there exists $\tilde{x} \in [x_* - \mu, 1 - \mu]$, $\tilde{e}(\tilde{x}) = 0$. In particular, in that case $c \notin \partial\mathcal{C}_{u_0,e_0}$. □

We can now show that Ψ defined in (1.8) is continuous.

PROPOSITION 2.4. — *The map Ψ is continuous on $\mathcal{C}_{u_0,e_0}$ and can be extended to $\overline{\mathcal{C}_{u_0,e_0}}$ as a continuous map denoted again Ψ.*

Proof. — The fact that Ψ is continuous on $\mathcal{C}_{u_0,e_0}$ follows from continuous dependence on parameters of solutions of an ODE (and the fact that the map Φ defined in (2.1) is locally Lipschitz). We consider now $c = (c_1, c_2) \in \partial\mathcal{C}_{u_0,e_0}$. Proposition 2.1 shows the maximal solution (u, e) of (1.5)-(1.6) is defined and continuous on $[0, 1)$ and can be extended continuously to 1 with $e(1) = 0$ and $u(1) \geqslant 0$. Therefore, we can define $\Psi(c) = (u(1), 0)$. If $u(1) > 0$, (u, e) is defined on an interval that strictly contains $[0, 1]$ and by continuous dependence on parameters, Ψ is continuous at c. We now have to deal with the case $u(1) = 0$. Lemma 2.2(iii) shows that c_1, $c_2 < 0$. Consider $\varepsilon > 0$. Let $\tilde{c} \in \overline{\mathcal{C}_{u_0,e_0}}$ close enough to c and denote by $(\tilde{u}, \tilde{e})$ the maximal solution of Problem (1.5)-(1.6) associated to $\tilde{c}$. By continuity of (u, e) there exists $x_* \in (0, 1)$ such that $0 < u(x_*), e(x_*) \leqslant \frac{\varepsilon}{2}$. Then, by continuous dependence on parameters, for any $\tilde{c}$ close enough to c, we have $0 < \tilde{u}(x_*), \tilde{e}(x_*) \leqslant \varepsilon$. Finally, by taking ε small enough, Remark 2.3 and the fact that $\tilde{u}$ is continuous at 1 give $0 < \tilde{u}(1) \leqslant M\varepsilon$ (where M depends only on c and Γ). Hence, Ψ is continuous at c. □

3. EXISTENCE

We are now ready to study existence. We first show that Ψ is "proper" in the following sense.

PROPOSITION 3.1. — *Assume that $u_0 > 0, e_0 > 0$ are fixed. Let $c = (c_1, c_2) \in \mathbb{R}^2$, such that $|c| \gg 1$ and denote by (u, e) the maximal solution of* (1.5)-(1.6). *Then, if $c \in \mathcal{C}_{u_0,e_0}$, either $u(1) \gg 1$, $e(1) \gg 1$ or $0 < u(1) \ll 1$.*

Proof. — Several situations can happen.
Case (i) ($c_1 \gg 1$). If $c \in \mathcal{C}_{u_0,e_0}$, $\frac{\alpha}{u_0} u' \geqslant c_1 + u_0$ and $u(1) \geqslant \frac{u_0}{\alpha}(c_1 + u_0) + u_0 \gg 1$.
Case (ii) ($c_2 \ll -1$). We consider the energy $y = \frac{\alpha}{2u_0} u^2 + \frac{\nu}{u_0} e$. Then,

$$y' = c_2 + (\Gamma + 1)e + \frac{u^2}{2} \leqslant c_2 + My$$

where M is a positive constant depending only on Γ, u_0, α, ν. Then, for any x in the domain of definition of y,

$$y(x) \leqslant y(0)e^{Mx} + \frac{c_2}{M}(e^{Mx} - 1),$$

so that if $c_2 < -\frac{M}{e^M-1}y(0)e^M$, e must vanish at a point between 0 and 1 and $c \notin \mathcal{C}_{u_0,e_0}$.

Case (iii) ($c_2 \gg 1$). Let $c \in \mathcal{C}_{u_0,e_0}$. We consider again the energy $y = \frac{\alpha}{2u_0}u^2 + \frac{\nu}{u_0}e$. Then,

$$y' = c_2 + (\Gamma+1)e + \frac{u^2}{2} \geqslant c_2 + my$$

where m is a constant depending only on Γ, u_0, α, ν. Therefore either $e(1) \gg 1$ or $u(1) \gg 1$.

Case (iv) ($c_1 \ll -1$ and $c_2 \leqslant \sqrt{-c_1}$) Let $c \in \mathcal{C}_{u_0,e_0}$. Using again $y = \frac{\alpha}{2u_0}u^2 + \frac{\nu}{u_0}e$ and following case (ii), we get $y' \leqslant -c_1 + My$ on $[0,1]$. Therefore, for $c_1 \ll -1$, there exists a constant B depending only on $u_0, e_0, \alpha, \nu, \Gamma$ such that $e \leqslant B\sqrt{-c_1}$ on $[0,1]$. Using this fact on the u-equation of System (1.5), we get

$$\frac{\alpha}{u_0}u' \leqslant c_1 + u + \frac{\Gamma B\sqrt{-c_1}}{u}.$$

Note that for $x \in [0,1]$, if $u(x) \in \left[-\frac{c_1}{4} - \frac{1}{2}\sqrt{\frac{1}{4}c_1^2 - 4\Gamma B\sqrt{-c_1}}, -\frac{c_1}{4} + \frac{1}{2}\sqrt{\frac{1}{4}c_1^2 - 4\Gamma B\sqrt{-c_1}}\right]$, then $\frac{\alpha}{u_0}u'(x) \leqslant \frac{1}{2}c_1$ and denote $b = -\frac{c_1}{4} - \frac{1}{2}\sqrt{\frac{1}{4}c_1^2 - 4\Gamma B\sqrt{-c_1}}$. We then notice that, for $c \in \mathcal{C}_{u_0,e_0}$ and $c_1 \ll -1$, u rapidly goes under b and stays under b. Therefore $u(1) \leqslant b \leqslant \frac{4\Gamma B}{\sqrt{-c_1}}$ and $u(1) \ll 1$. □

Remark 3.2. — We proved in the previous proposition that there exists a constant $A > 0$ depending only on $u_0, e_0, \alpha, \nu, \Gamma$ such that for any $c_2 \leqslant -A$, $c \notin \mathcal{C}_{u_0,e_0}$ (see case(ii)). Note also that if $\frac{\nu}{u_0}e_0 + c_2 - c_1u_0 - \frac{1}{2}u_0^2 + e_0 \leqslant 0$ and $c_1 + u_0 \geqslant 0$, then $c \notin \mathcal{C}_{u_0,e_0}$. Indeed, in this case, u increases and $-c_1u - \frac{1}{2}u^2 \leqslant -c_1u_0 - \frac{1}{2}u_0^2$ so that e is decreasing, $e' \leqslant -e_0$ and then e crosses 0 in $(0,1]$.

The previous proposition is not empty in the sense that $\mathcal{C}_{u_0,e_0}$ is not bounded.

LEMMA 3.3. — *Assume $u_0 > 0, e_0 > 0$ are fixed. There exists a positive number A depending only on $\Gamma, u_0, e_0, \alpha, \nu$ such that if $c_1 + u_0 + \frac{\Gamma A(|c_2|+1)}{u_0} < 0$ and $c_2 + e_0 > 0$, then $(c_1, c_2) \in \mathcal{C}_{u_0,e_0}$.*

Proof. — For $c = (c_1, c_2)$, we denote by (u, e) the maximal solution of Problem (1.5)-(1.6) and by I its interval of definition. Following case (ii) in the previous proposition there exists a constant $A > 0$ depending only on $\Gamma, u_0, e_0, \alpha, \nu$ such that $e \leqslant A(|c_2| + 1)$ on $[0,1] \cap I$. Then we note that since $c_1 < c_1 + u_0 < 0$, the map $y \in [0, u_0] \mapsto -c_1y - \frac{1}{2}y^2$ is nonnegative so that for any $x \in [0,1] \cap I$ such that $0 < u(x) \leqslant u_0$, we have $\frac{\nu}{u_0}e'(x) \geqslant c_2 + e(x)$. Note also that for $x \in [0,1] \cap I$ such that $u(x) = u_0$,

$$\frac{\alpha}{u_0}u'(x) \leqslant c_1 + u_0 + \Gamma\frac{A(|c_2|+1)}{u_0} < 0.$$

In particular $u'(0) < 0$, $e'(0) > c_2 + e_0 > 0$ and $\{x \in (0,1] \cap I\ ,\ u(x) = u_0\}$ is empty. By Lemma 2.2(i)-(ii), $[0,1] \subset I$, e is increasing and $0 < u \leqslant u_0$ on $[0,1]$so that $c \in \mathcal{C}_{u_0,e_0}$. □

We now define for $\varepsilon > 0$, $E_\varepsilon = \{(x,y) \in \mathbb{R}^2\ ,\ \varepsilon < x, y < \frac{1}{\varepsilon}\}$ and $\Omega_\varepsilon = \Psi^{-1}(E_\varepsilon)$. By continuity of Ψ (Proposition 2.4) and Proposition 3.1, Ω_ε is open, bounded and $\overline{\Omega_\varepsilon} \subset \mathcal{C}_{u_0,e_0}$. We denote by Ψ_ε the restriction of Ψ to Ω_ε, and by $d(\Psi_\varepsilon, \Omega_\varepsilon, (e_1, u_1))$

the Brouwer degree [16, 34, 22, 35, 17] of Ψ_ε in Ω_ε with respect to the target (e_1, u_1)).

Recall, for *regular values* (e_1, u_1), defined as values for which Ψ_ε is differentiable and full rank on $\Psi_\varepsilon^{-1}(e_1, u_1)$,

$$d(\Psi_\varepsilon, \Omega_\varepsilon, (e_1, u_1)) := \sum_{c \in \Psi_\varepsilon^{-1}(e_1, u_1)} \operatorname{sgn} \det d\Psi_\varepsilon(c), \tag{3.1}$$

that is, the degree counts roots with sign depending on orientation. For arbitrary (not necessarily regular) values (e_1, u_1) for which $\Psi_\varepsilon^{-1}(u_1, e_1) = \emptyset$, $d(\Psi_\varepsilon, \Omega_\varepsilon, (e_1, u_1)) = 0$. Thus, *nonzero Brouwer degree implies existence of a solution.* Finally, recall that $d(\Psi_\varepsilon, \Omega_\varepsilon, (e_1, u_1))$ is homotopy invariant, so long as $\Psi_\varepsilon^{-1}(e_1, u_1)$ remains disjoint from $\partial\Omega_\varepsilon$. Typically, degree is evaluated at a regular value, then deduced for other values by homotopy invariance.

COROLLARY 3.4. — *Assume that $u_0 > 0$ and $e_0 > 0$ are fixed. Let $u_1 > 0$, $e_1 > 0$. Then for $\varepsilon > 0$ small enough, $(u_1, e_1) \notin \Psi(\partial\Omega_\varepsilon)$ and the Brouwer degree $d(\Psi_\varepsilon, \Omega_\varepsilon, (e_1, u_1))$ is independent of (u_1, e_1) and ε.*

Proof. — Let $u_1 > 0, e_1 > 0$. First, Proposition 3.1 shows that $\Psi^{-1}(u_1, e_1)$ is bounded and included in the open set Ω_ε for ε small enough. In particular, $d(\Psi_\varepsilon, \Omega_\varepsilon, (e_1, u_1))$ is independent of ε small enough. Furthermore, we also get from Proposition 3.1 that for any $t \in [0, 1]$, $(1 + (1-t)u_1, 1 + (1-t)e_1) \notin \Psi(\partial\Omega_\varepsilon)$ if ε is small enough. Hence, by homotopy invariance, $d(\Psi_\varepsilon, \Omega_\varepsilon, (e_1, u_1))$ and $d(\Psi_\varepsilon, \Omega_\varepsilon, (1, 1))$ are equal. □

At this point we make use of the fundamental property that gas dynamics has an associated convex entropy $\eta(\rho, \rho u, \rho E)$ in the sense of [29, 26], namely $\eta = -\rho S$, where $S(\rho^{-1}, e)$ is thermodynamic entropy; see [26, §4]. That is, writing (1.1) as $U_t + f(U)_x = (B(U)U_x)_x$, where $U = (\rho, \rho u, \rho E)^t$, there hold: for any $U \in \mathbb{R}^3$, the Hessian matrix $d^2\eta_U > 0$; $d\eta_U \circ df_U = dq_U$ for some flux q; and $d^2\eta_U B(U)$ is symmetric positive semidefinite, hence $\langle V, d^2\eta_U B(U)V\rangle \leqslant 0$, with equality if and only if $d^2\eta_U B(U)V = 0$, or equivalently $B(U)V = 0$. Composing the equations on the left by $d\eta$, we have

$$\begin{aligned} \eta(U)_t + q(U)_x &= d\eta_U(B(U)U_x)_x = (d\eta_U(B(U)U_x))_x - \langle d^2\eta_U U_x, B(U)U_x\rangle \\ &= (d\eta_U(B(U)U_x))_x - \langle U_x, d^2\eta_U B(U)U_x\rangle, \end{aligned} \tag{3.2}$$

giving $\eta(U)_t + q(U)_x - (d\eta_U(B(U)U_x))_x \leqslant 0$ with equality if and only if $B(U)U_x = 0$. Using the definition $B(U)U_x = (\alpha u_x, \kappa T_x + \alpha u u_x)^t$ given by (1.1), we find that $B(U)U_x = 0$ is equivalent to $(u, T)_x = 0$, and therefore to $(u, e)_x = 0$. Integrating the time-independent profile equation from $x = 0$ to 1, we thus obtain

$$\left[q(\hat{U}) - d\eta_{\hat{U}}(B(\hat{U})\hat{U}_x)\right]_0^1 \leqslant 0, \text{ with equality if and only if } (\hat{u}, \hat{e}) \equiv \text{constant}. \tag{3.3}$$

LEMMA 3.5. — *For steady gas dynamics on an interval, (1.1)–(1.2), with constant boundary conditions $(u_0, e_0) = (u_1, e_1)$, the unique global solution is given by the constant solution $(\hat{\rho}, \hat{u}, \hat{e}) \equiv (\rho_0, u_0, e_0)$. Equivalently $c_* = (-u_0 - \Gamma e_0/u_0, -(1+\Gamma)e_0 - u_0^2/2)$ is the unique global solution of $\Psi(c) = (u_1, e_1)$; moreover, it is nondegenerate, with $\operatorname{sgn}\det d\Psi(c_*) = +1$.*

Proof. — From $\hat{\rho}\hat{u} =: m \equiv$ constant, we obtain $(\rho, u, e)(0) = (\rho, u, e)(1)$, or $U(0) = U(1)$ in the vectorial notation above. Note that η may be modified by the

addition of any affine function while preserving its properties as a convex entropy (by changing q accordingly). Thus, by an appropriate affine shift, we may arrange that $\eta(U(0)) = 0$ and $d\eta_{U(0)} = 0$, so that the left-hand side vanishes in (3.3) (since $\eta(U(0)) = \eta(U(1))$ and $d\eta_{U(0)} = d\eta_{U(1)}$), and therefore $(\hat{u}, \hat{e}) \equiv$ constant. But, then, $\hat{\rho} = m/\hat{u} \equiv$ constant as well, and so $(\hat{\rho}, \hat{u}, \hat{e}) \equiv (\rho_0, u_0, e_0)$ as claimed. The computation of $d\Psi(c^*)$ amounts to integration of a 2×2 constant-coefficient linearized equations about this constant solution, hence may be carried out explicitly to find that $\operatorname{sgn} \det d\Psi(c_*) = +1$. We omit this calculation as we will show it in a simpler and more general way later on. See Subsection 5.1. □

Remark 3.6. — Lemma 3.5 may be recognized as a particularly concrete instance of results stated for general systems in [33, Thm 2.10] and [33, Prop. 2.9]. In particular, $\operatorname{sgn} \det d\Psi(c_*) = +1$ is seen by abstract considerations to hold for constant solutions of general symmetrizable systems, without explicit calculation. We note for gas dynamics that the key identity (3.2) may be obtained readily from the thermodynamic relation $de = T\,dS + p\,dv$ defining S, where $V = 1/\rho$, or $S_t = T^{-1}(e_t - pv_t)$, together with (1.1), without verifying convexity or symmetrizability, with no need to invoke general theory.

THEOREM 3.7 (Large-data existence). — *For steady gas dynamics on an interval,* (1.1)–(1.2)*, there is at least one steady solution for every choice of left and right data.*

Proof. — Applying Corollary 3.4, we find that the Brouwer degree is independent of the target (u_1, e_1). Thus we may compute the degree at the constant data $(u_1, e_1) = (u_0, e_0)$. By Lemma 3.5, $\Psi^{-1}(u_1, e_1)$ consists of the single point $c_* = (-u_0 - \Gamma e_0/u_0, -(1+\Gamma)e_0 - u_0^2/2)$, at which $\operatorname{sgn} \det d\Psi(c_*) = +1$. Thus, by (3.1), the degree at (u_1, e_1) is $+1$. This implies that the Brouwer degree is $+1$ for all values of the target, implying existence of a solution. □

4. Uniqueness

We next characterize uniqueness, by a global version of the local [3, Lemma 3.10].

PROPOSITION 4.1. — *If $\gamma := \det d\Psi(c)$ does not vanish on the feasible set $\mathcal{C}_{u_0,e_0}$, then solutions of* (1.9) *are globally unique for each choice of data $(\rho_0, u_0, e_0, u_1, e_1)$. If on the other hand γ changes sign on the feasible set $\mathcal{C}_{u_0,e_0}$, then even local uniqueness is violated; in particular, there is at least one choice of data possessing multiple solutions.*

Proof. — Nonvanishing of γ implies nonvanishing of the Jacobian determinant $\det d\Psi(c)$, which implies $d\Psi(c)$ full rank and $\operatorname{sgn} \det d\Psi(c) \equiv +1$ for all c. In particular every values are regular and it follows that the degree of Ψ with respect to a target (u_1, e_1) is equal to $+n$, where n is the number of solutions for that data. Since we have already shown that degree is identically equal to $+1$, this is a contradiction unless roots are unique i.e., $n = 1$. This proves the first assertion. For the second assertion, just notice that uniqueness implies that degree is equal to the sign of γ at the unique solution and therefore a change of sign in γ implies a change in degree. Hence, by contradiction, uniqueness is impossible when γ changes sign. □

Conclusion: *Uniqueness or nonuniqueness hinges on nonvanishing of* $\det d\Psi(\cdot)$ *on* $\mathcal{C}_{u_0,e_0}$.

5. Spectral stability and the Evans function

We can reduce Problem (1.1) to

$$\begin{aligned}
&\rho_t + (\rho u)_x = 0\,,\\
&\rho u_t + \rho u u_x + (\Gamma \rho e)_x = \alpha u_{xx}\,,\\
&\rho e_t + \rho u e_x + \Gamma \rho e u_x = \nu e_{xx} + \alpha u_x^2\,,
\end{aligned}$$

from which we obtain the eigenvalue problem around a steady state $(\hat\rho, \hat u, \hat e)$

$$\begin{aligned}
&\lambda\rho + (\hat\rho u + \hat u\rho)_x = 0\,,\\
&\lambda\hat\rho u + (\hat\rho\hat u u + \Gamma\hat\rho e + \Gamma\hat e\rho)_x + \hat u_x\,(\hat\rho u + \hat u\rho) = \alpha u_{xx}\,,\\
&\lambda\hat\rho e + (\hat\rho\hat u e)_x + \hat e_x\,(\hat\rho u + \hat u\rho) + \Gamma\hat\rho\hat e u_x + \Gamma\hat u_x\,(\hat\rho e + \hat e\rho) = \nu e_{xx} + 2\alpha\hat u_x u_x\,,
\end{aligned} \tag{5.1}$$

with boundary conditions

$$(\rho, u, e)(0) = 0,\ (u, e)(1) = 0. \tag{5.2}$$

Note that for $\lambda = 0$ the previous system can be written in the alternative form

$$\begin{aligned}
&\hat\rho u + \hat u\rho = 0\,,\\
&(\hat\rho\hat u u + \Gamma\hat\rho e + \Gamma\hat e\rho)_x = \alpha u_{xx}\,,\\
&\big((1+\Gamma)\hat\rho\hat u e + \hat\rho\hat u^2 u\big)_x = \nu e_{xx} + \alpha\,(\hat u u_x + \hat u_x u)_x\,.
\end{aligned} \tag{5.3}$$

We are using here the standard approach [1, 20] of rewriting (5.1) as a first-order system and a Cauchy problem. Note that, after eliminating ρ, (5.1) may be rewritten as a first-order system in (u, e, u', e'), following the standard approach of [1, 20], with homogeneous data prescribed on (u, e) at both ends. The *Evans function* may thus be defined via a "shooting" construction, similarly as in [36, 37] for the half-line case, as

$$D(\lambda) := \det \begin{pmatrix} u_1(1) & u_2(1) \\ e_1(1) & e_2(1) \end{pmatrix}, \tag{5.4}$$

where (ρ_j, u_j, e_j) are solutions of (5.1) with initial conditions

$$(\rho_1, u_1, e_1, u_1', e_1')(0) = (0,0,0,1,0), \quad (\rho_2, u_2, e_2, u_2', e_2')(0) = (0,0,0,0,1);$$

that is, as the Wronskian at $x = 1$ of a basis of solutions satisfying the boundary conditions at $x = 0$. This Wronskian vanishes precisely when there exists a solution vanishing in (e, u) at both $x = 0, 1$, i.e., an eigenfunction. Evidently, $D(\cdot)$ is analytic in λ on all of $\mathbb{C}$, and real-valued for λ in $\mathbb{R}$, with zeros corresponding to eigenvalues of the linearized operator about the associated steady solution.[1]

Conclusion: *Spectral stability is equivalent to nonvanishing of* D *on* $\{\Re\lambda \geqslant 0\}$.

[1] Indeed, as standard in Evans function theory, zeros correspond in both location and multiplicity to eigenvalues of the linearized operator about the wave; see, e.g., [1, 20, 42] in the whole-line case.

5.1. **The stability index.** Clearly D is real-valued for real λ. It is readily seen (see, e.g. [32]) that $D(\lambda) \neq 0$ for λ real and sufficiently large, hence we may define as in [20] the *Stability index*

$$\mu := \mathrm{sgn} D(0) \left(\lim_{\lambda \to +\infty_{real}} \mathrm{sgn} D(\lambda) \right)$$

as a nonvanishing multiple $\pm \mathrm{sgn} D(0)$ of $\mathrm{sgn} D(0)$. Evidently, μ determines the parity of the number of roots of the Evans function with positive real part, or, equivalently (since complex roots occur in conjugate pairs), the number of positive real roots, with $+1$ corresponding to "even" and -1 to "odd". As such, it is often useful in obtaining *instability* information.

Moreover, we have the following key observation relating the low-frequency stability and the stability index information to transversality of the steady profile solution of the standing-wave ODE.

LEMMA 5.1. — *The zero-frequency limit $D(0)$ is equal to $\frac{\alpha\nu}{u_0^2}$ multiplied by the Jacobian determinant $\det d\Psi(c)$ associated with problem (1.9) evaluated at any root c; in particular,*

$$\mathrm{sgn} D(0) = \mathrm{sgn} \det d\Psi(c). \tag{5.5}$$

Proof. — The proof amounts to the observation that the operations of linearization and integration of the standing-wave ODE commute. Taking the variation of the profile equation (1.5) with respect to c gives

$$\begin{aligned} &\frac{\alpha}{u_0}\dot{u}' = \dot{c}_1 + \dot{u} + \Gamma\left(\frac{\dot{e}}{\hat{u}} - \frac{\hat{e}}{\hat{u}^2}\dot{u}\right), \\ &\frac{\nu}{u_0}\dot{e}' = \dot{c}_2 - (\dot{c}_1\hat{u} + c_1\dot{u}) - \hat{u}\dot{u} + \dot{e}, \\ &(\dot{u}, \dot{e})(0) = (0,0), \end{aligned} \tag{5.6}$$

where $\dot{}$ denotes variation. Furthermore, we deduce from relations (1.7) that

$$(\dot{c}_1, \dot{c}_2) = \left(\frac{\alpha}{u_0}\dot{u}'(0), \frac{\nu}{u_0}\dot{e}'(0) + \alpha\dot{u}'(0)\right).$$

It is readily verified for $\lambda = 0$ that the eigenvalue equations (5.3) can be integrated from 0 to x to yield the same system (5.6) (note that $\hat{\rho}\hat{u} = u_0$). Therefore, keeping the notations of (5.4), for $(\dot{c}_1, \dot{c}_2) = (1,0)$, $(\dot{u}, \dot{e}) = \frac{u_0}{\alpha}(u_1, e_1) - \frac{u_0^2}{\nu}(u_2, e_2)$, whereas for $(\dot{c}_1, \dot{c}_2) = (0,1)$, $(\dot{u}, \dot{e}) = \frac{u_0}{\nu}(u_2, e_2)$. The result follows. □

Remark 5.2. — The previous lemma gives us another way to compute $D(0)$. Considering the problem

$$\begin{aligned} &\frac{\alpha}{u_0}u' = d_1 + \left(1 - \Gamma\frac{\hat{e}}{\hat{u}^2}\right)u + \frac{\Gamma}{\hat{u}}e, \\ &\frac{\nu}{u_0}e' = d_2 - d_1\hat{u} - \frac{\alpha}{u_0}\hat{u}'u + e + \Gamma\frac{\hat{e}}{\hat{u}}u, \\ &u(0) = 0, e(0) = 0, \end{aligned} \tag{5.7}$$

we have

$$D(0) = \det \begin{pmatrix} u_1(1) & u_2(1) \\ e_1(1) & e_2(1) \end{pmatrix}$$

where (u_1, e_1) solves (5.7) for $(d_1, d_2) = \left(\frac{\alpha}{u_0} - u_0 - \Gamma\frac{e_0}{u_0}, \alpha - e_0 - \frac{1}{2}u_0^2 - \Gamma e_0\right)$ and (u_2, e_2) solves (5.7) for $(d_1, d_2) = \left(-u_0 - \Gamma\frac{e_0}{u_0}, \frac{\nu}{u_0} - e_0 - \frac{1}{2}u_0^2 - \Gamma e_0\right)$ (see (1.7) for the link between (c_1, c_2) and $(u'(0), e'(0))$).

Remark 5.3. — Lemma 5.1 is analogous to the Zumbrun-Serre/Rousset lemmas of [43, 36] in the whole- and half-line case, which say $D(\lambda) \sim \gamma\delta(\lambda)$ for $|\lambda| \ll 1$, where γ is a Wronskian encoding transversality of the associated standing-wave ODE and δ is a Lopatinski determinant for the inviscid stability problem (here trivially nonvanishing).

Conclusion: Both Brouwer degree $\gamma = \operatorname{sgn}\det d\Psi(\cdot)$ and stability index μ are determined by $\operatorname{sgn}(D(0))$, hence (by Proposition 4.1 and the discussion just above) uniqueness and topological stability information may be obtained by evaluation of $D(0)$ on the feasible set $\mathcal{C}_{u_0,e_0}$. In particular, differently from the cases of the whole- or half-line (see, e.g., the discussion of [40, §6.2]), *changes in stability/Morse index associated with passage of a single eigenvalue through $\lambda = 0$ are necessarily associated with bifurcation/nonuniqueness.*

6. Numerical investigations

For simple gases, the ratio $\frac{\nu}{\alpha}$ follows closely to the prediction

$$\frac{\nu}{\alpha} = \frac{27\Gamma + 12}{16} \tag{6.1}$$

of statistical mechanics [23, 24].[2] In our numerics, we will assume, further, (6.1).

6.1. **Feasible set.** For our numerical studies, we rescale equation (1.1) through the following change of coordinates, $\rho = \rho_0\bar{\rho}$, $u = u_0\bar{u}$, $e = u_0^2\bar{e}$, $t = \frac{\bar{t}}{u_0}$, $\bar{\alpha} := \frac{\alpha}{\rho_0 u_0}$, $\bar{\nu} := \frac{\nu}{\rho_0 u_0}$, which allows us to always fix $\rho_0 = u_0 = 1$. We note that the assumption concerning the ratio of viscosities for simple gases still holds under this change of coordinates, $16\bar{\nu} = \bar{\alpha}(27\Gamma + 12)$. Hereafter, we drop the bar notation. To map out the feasible set, we solve the profile equation (1.5) (with $u_0 = 1$) as an initial value problem on the interval $[0, 1]$ with initial conditions $(u, e)(0) = (1, e_0)$ for various values of the integration constants c_1, c_2. We center the map about the integration constants corresponding to the fixed point, $c_1 = -1 - \Gamma e_0$, $c_2 = -\frac{1}{2} - (1+\Gamma)e_0$. We check to ensure that u and e remain positive throughout the unit interval and that finite blowup does not occur; see Appendix A.1 for details about computational algorithms. In Figure 6.1, we plot some examples of the feasible set. Note that the feasible set is unbounded (see Lemma 3.3).

We tested the following parameters to see if they lie in the feasibility set,

$$\begin{aligned}(\Gamma, \alpha, e_0, \Delta c_1, \Delta c_2) \in \{2/3, 2/5, 1\} \times \operatorname{lin}(0.1, 2, 10) \times \operatorname{lin}(0.001, 10, 30)\\ \times \operatorname{lin}(-50, 50, 50) \times \operatorname{lin}(-50, 50, 50),\end{aligned}$$

where $\operatorname{lin}(a, b, c)$ indicates the set containing c evenly spaced points in the interval $[a, b]$, $\nu = \frac{\alpha(27\Gamma+12)}{16}$, and $c_1 = -1 - \Gamma e_0 + \Delta c_1$, $c_2 = -\frac{1}{2} - (1+\Gamma)e_0 + \Delta c_2$.

[2] In the notation of [24], $\alpha = 2\mu + \eta = \frac{4}{3}\mu$, $\gamma = \Gamma + 1$, and $\frac{\kappa}{c_v\mu} = \frac{9\gamma-5}{4}$, giving the result.

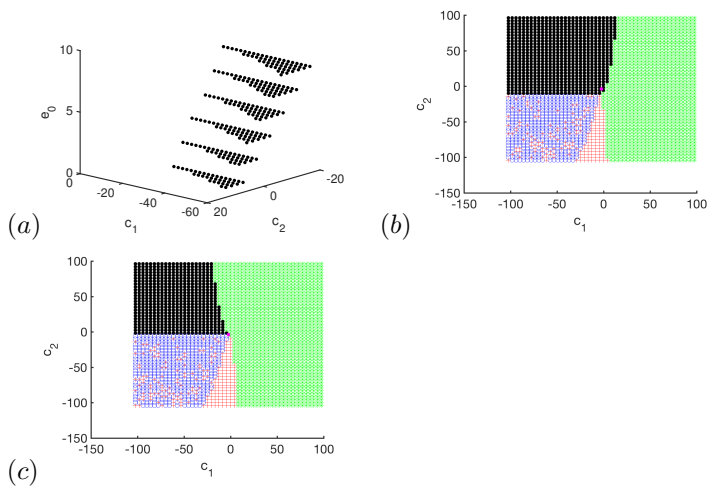

FIGURE 6.1. (a) Plot of the feasible set as e_0 varies when $\Gamma = 1$, $\alpha = 0.1$, and $\nu = 0.244$. (b) Plot of the feasible set with black dots, the set where u goes negative on $[0, 1]$ with blue circles, the set where e goes negative on $[0, 1]$ with green stars, and the set where there is finite time blowup on $[0, 1]$ with red $+$ signs for $\alpha = 2$, $\nu = 3.75$, $\Gamma = 2/3$, $e_0 = 2$. (c) Plot of the feasible set with black dots, the set where u goes negative on $[0, 1]$ with blue circles, the set where e goes negative on $[0, 1]$ with green stars, and the set where there is finite time blowup on $[0, 1]$ with red $+$ signs for $\alpha = 0.2$, $\nu = 1$, $\Gamma = 2/3$, $e_0 = 2$. A bold magenta dot marks the constant solution on plots (b) and (c).

6.2. **Evans function computations.** To numerically compute the Evans function, we use the package STABLAB [9], which is well tested by this point; for example see [6, 11, 12]. We provide details about numerical conditioning and algorithm choices we use in STABLAB in Appendix A.2.

6.3. **Winding number computations.** To test for the existence of unstable eigenvalues, we compute the Evans function on a contour consisting of the boundary ∂S of the set $S := \{z \in B(0, 100) : \Re(z) \geqslant 0\}$. We use the functionality built into STABLAB [9] that adaptively chooses the mesh along ∂S so that the relative error between any two consecutive points on the image of ∂S under the Evans function, C_S, varies by no more than 0.2. We then compute the winding number of C_S, which is the number of eigenvalues of (5.1) inside S. In Figure 6.2, we demonstrate the profile and corresponding Evans function computation for representative parameters.

We compute the Evans function on the contour ∂S for the parameters, if they are in the feasible set, given by

$$(\Gamma, \alpha, e_0, \Delta c_1, \Delta c_2) \in \{2/3, 2/5, 1\} \times \text{lin}(0.1, 2, 10) \times \text{lin}(0.001, 10, 30) \times \text{lin}(-50, 50, 50) \times \text{lin}(-50, 50, 50),$$

where $\text{lin}(a, b, c)$ indicates the set containing c evenly spaced points in the interval $[a, b]$, $\nu = \frac{\alpha(27\Gamma+12)}{16}$, $c_1 = -1-\Gamma e_0+\Delta c_1$, and $c_2 = -\frac{1}{2}-(1+\Gamma)e_0+\Delta c_2$. In all, we computed the Evans function on 670,926 contours, and in all cases found the winding number to be zero. These computations took the equivalent of approximately 83.8 computation days on a desktop with 10 duo cores.

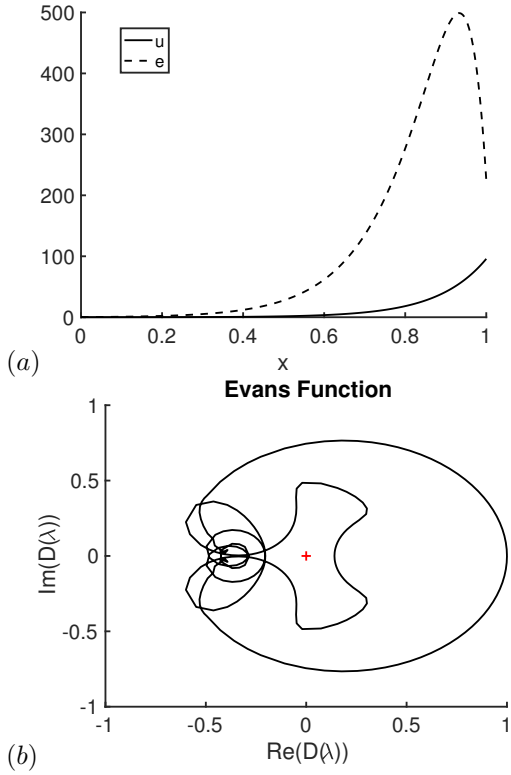

FIGURE 6.2. For the parameters $\alpha = 0.1$, $\Gamma = 1$, $\nu = 0.2438$, $e_0 = 0.001$, $c_1 = -18.35$, and $c_2 = 0.5184$, we plot (a) the boundary layer profile, and (b) the image of $S := \{z \in B(0, 100) : \Re(z) \geqslant 0\}$ under the Evans function. The winding number is zero indicating spectral stability of the boundary layer profile.

6.4. **Computations in original coordinates.** As mentioned at the beginning of Section 6, we use a convenient scaling for the numerics. To give an idea of the region studied in the original coordinates corresponding to the analytical results, we provide the following plots. In Figure 6.3 (a), we plot the coordinates for the initial data, and in Figure 6.3 (b) we plot the coordinates for the final data, for the

profiles for which existence is shown. In Figures 6.3 (c) and (d), we plot the same initial and final profile data for which we were able to compute the Evans function and show stability. We note that computing the Evans function is very challenging due to stiffness of the associated ODEs.

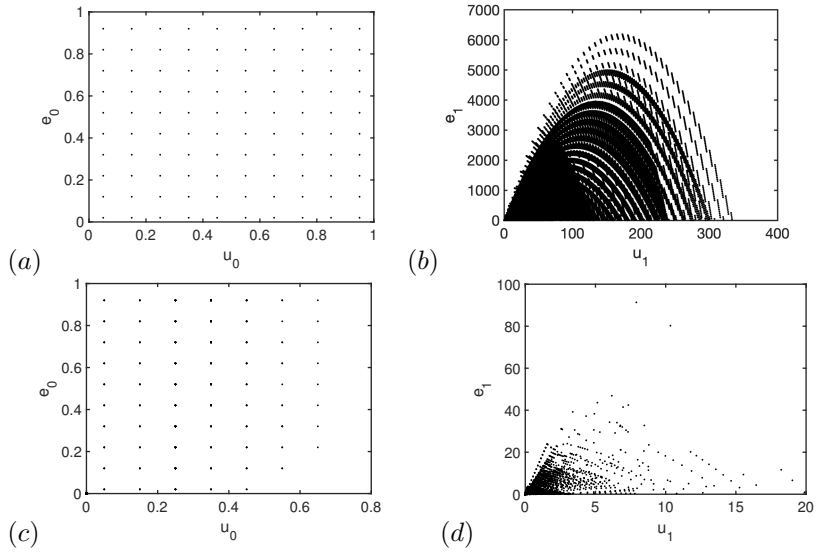

FIGURE 6.3. (a) Plot of initial conditions (u_0, e_0) considered. (b) Plot of resulting (u_1, e_1) end conditions when $\Gamma = 2/3$ and $-50 \leqslant c_1 \leqslant 50$ (approximately 50 points) and $-50 \leqslant c_2 \leqslant 50$ (approximately 200 points). In Figures (c) and (d) we plot the profile data for which we were able to compute the Evans function.

6.5. **Global uniqueness/stability index.** For the parameters in the feasible set described in Section 6.1, we computed the Evans function at the origin, $D(0)$. We found that the smallest value of $D(0)$ for the computed parameters is 4.19e-4. Thus, $D(0)$ appears not to vanish on the feasible set, confirming global uniqueness; likewise, the stability index $\mu \equiv +1$. See Figure 6.4 for a demonstration of how $D(0)$ varies as c_1 and c_2 vary in the feasible set.

7. A NUMERICAL COUNTEREXAMPLE

We now consider equations (1.1) subject to the equation of state $\bar{e}(\tau, S) = \frac{e^S}{\tau} + S + \frac{\tau^2}{2}$ considered in [3], where τ corresponds to specific volume and S corresponds to entropy. Specific density is given by $\rho = \frac{1}{\tau}$, and $T = \bar{e}_S = \frac{e^S}{\tau} + 1$, so $e^S = \frac{T-1}{\rho}$, or

$$S = \hat{S}(\rho, T) = \ln\left(\frac{T-1}{\rho}\right). \tag{7.1}$$

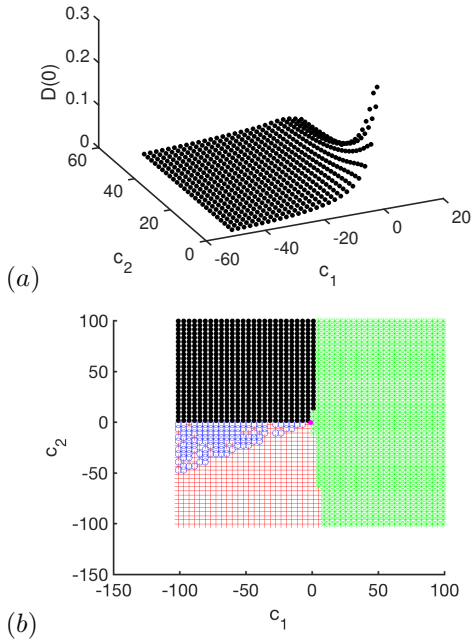

FIGURE 6.4. In these figures, $\alpha = 0.7\bar{3}$, $\Gamma = 2/3$, $\nu = 1.375$, and $e_0 = 0.001$. (a) Plot of $D(0)$ against c_1 and c_2. (b) Plot of the feasible set corresponding to Figure (a) with black dots, the set where u goes negative on $[0,1]$ with blue circles, the set where e goes negative on $[0,1]$ with green stars, and the set where there is finite time blowup on $[0,1]$ with red + signs.

From this, we obtain

$$\begin{aligned} p = \hat{p}(\rho, T) &= -\bar{e}_\tau = \rho(T-1) - \frac{1}{\rho}, \\ e = \hat{e}(\rho, T) &= T - 1 + \ln\left(\frac{T-1}{\rho}\right) + \frac{1}{2}\rho^2, \end{aligned} \tag{7.2}$$

closing the system, together with the energy relation $E = e + \frac{1}{2}u^2$, in terms of variables (ρ, u, T), $T > 1$. Alternatively, inverting the relation $e = \hat{e}(T, \rho)$ using $\hat{e}_T > 0$ for $T > 1$, we may consider it as implicitly determining a system in the usual variables (ρ, u, e), with $e > 0$. This is the system referred to as the *local model* in [3]. Notably, the function $\eta := -\rho\hat{S}(\rho, T)$, with $\hat{S}$ as in (7.1) considered as a function of the conservative variables $(\rho, \rho u, E)$ *is a convex entropy for system* (1.1) in the sense of [29, 26]; see [3].

In [3] it was shown that the local model considered on the whole line has unstable shock waves for parameters for which the inviscid system has stable waves. Here, we demonstrate that the local model considered on a finite interval has parameters for which uniqueness of solutions fails, and also other, nearby parameters for which a Hopf-bifurcation occurs.

These results are guided by the general principles of [41] relating spectra of standing shocks on the whole line to spectra of pieces thereof, considered as solutions on a truncated domain. See [33, §3.2] for further discussion in the specific case of a finite interval. The first relevant principle is that spectra on the interval are, for $\Re\lambda \geqslant 0$ and $\lambda \neq 0$ given in the limit as interval length goes to infinity- equivalently, as viscosity goes to zero- by the direct sum of spectra on the whole line together with spectra of constant boundary layers on the half-line with data corresponding to that on the left (resp. right) endpoint of the interval. This implies that strict instability on the whole line implies strict instability on the interval with associated stability transition as amplitude is increased from a (presumably stable; see [33, Proposition 3.2]) constant steady solution to an unstable one.

The second principle is that in the same large interval length/small viscosity standing-shock limit, the stability index does not vanish ([33, Prop. 3.3]), or equivalently $D(0) \neq 0$. Thus, if a homotopy is taken from stable constant solutions to unstable standing shock solutions, entirely within the class of standing shocks with sufficiently large interval/small viscosity, then the associated stability transition cannot correspond to a simple crossing of an eigenvalue through the origin $\lambda = 0$, as $D(0) \neq 0$, and must therefore involve the crossing of one or more pairs of complex conjugate roots, i.e., a Hopf-type scenario.

On the other hand, the first cited principle implies that two of these roots must be near the pair of roots at the origin of the whole-line shock as it undergoes transition to instability: one "translational" eigenvalue fixed at $\lambda = 0$ and the crossing eigenvalue corresponding to instability. Thus, we have the picture of a Hopf bifurcation with very nearby roots, i.e., with associated time-period going to infinity, a quite delicate scenario. This makes numerical verification somewhat sensitive; however, it also aids us in finding a more standard bifurcation in the form of a single crossing eigenvalue through $\lambda = 0$, as we are able to find by playing with the left and right boundaries of the interval for a given, sufficiently large-amplitude standing shock on the whole line.

7.1. **Nonuniqueness. Abstract bifurcation result** We first demonstrate (numerically) a bifurcation implying nonuniqueness. Namely, considering the restriction to a finite interval $[x_L, x_R]$, of an appropriate standing-shock solution of the local model on the whole line (described in detail below), we show that $D(0)$ changes sign as x_L and x_R vary; see Figure 7.3 (a)-(c). Defining by $c_*(x_L, x_R)$ the value of c corresponding to the shock profile on $[x_L, x_R]$, define the map

$$\Phi(c; x_L, x_R) := \psi(c_*(x_L, x_R) + c; x_L, x_R) - \psi(c_*(x_L, x_R); x_L, x_R),$$

where $\psi(x; x_L, x_R)$ is the solution map ψ associated with the interval $[x_L, x_R]$. Then $\Phi(0; x_L, x_R) \equiv 0$, reflecting the fact that the shock profile restricted to $[x_L, x_R]$ solves its own data. Existence of additional roots $c \neq 0$ for some x_L, x_R implies nonuniqueness for the same data. Nonuniqueness may be detected, therefore, using the following abstract bifurcation result, in the spirit of Proposition 4.1 and [3, Lemma 3.10].

PROPOSITION 7.1. — *Let $\Phi(c; p) : \mathbb{R}^m \times \mathbb{R}$ satisfy $\Phi(0; p) \equiv 0$. If $\gamma := \det(d\Phi(0; p))$ changes sign as p crosses a particular bifurcation value $p = p_*$, then $\Phi(\cdot; p)$ has a nontrivial root $c \neq 0$ for p arbitrarily close to p_*.*

Proof. — Arguing by contradiction, suppose that $c = 0$ is the unique root of $\Phi(c; p) = 0$ for p in a neighborhood of p_*. Thus, Φ does not vanish on the boundary of a small ball $B(0, r)$, hence the topological degree of $\Phi(\cdot; p)$ is independent of p. However, at p for which $\det(d\Phi(0; p)) > 0$, the degree is by the assumed uniqueness of roots equal to $+1$, while at points p for which $\det(d\Phi(0; p)) < 0$, the degree is -1, a contradiction. □

To show non-uniqueness, we first solve for the profile corresponding to the whole-line shock. Then we take the piece of that solution on $[x_L, x_R]$ as the profile for the finite boundary problem posed on the same interval. The computations showing non-uniqueness are relatively difficult. In the following discussion, $S_- := \lim_{x\to-\infty} S(x)$, is the left end state value of entropy in the whole-line shock wave solution of the local model. To solve for the profile, we fix the parameters $\alpha = \kappa = 1$ and take $S_- = 1$. From the Rankine-Hugoniot conditions, we obtain the other parameters. We then use a boundary value solver to obtain the whole-line viscous shock solution. Next, we use continuation with 30 evenly spaced steps in S_- to obtain the solution at $S_- = -5$. That is, we change the parameter S_- by a small amount and solve for the other parameters given by the Rankine-Hugoniot conditions, then use the profile solution corresponding to the previous value of S_- as an initial guess in the boundary value solver to solve for the profile for the new parameters. In solving for the whole-line profile, we use STABLAB which adaptively increases the spatial domain $[-L, L]$, $L \gg 1$, until the profile converges to the fixed-point end states, corresponding to the shock at $x = \pm\infty$, to within requested tolerance. To compute the Evans function, we used the same procedure as described in Section 6.2, except that we evaluate the Wronskian to obtain the Evans function at $x = 0$ instead of $(x_L + x_R)/2$, and we use "pseudo-Lagrangian coordinates" as described in [8] to reduce winding in our winding number studies without changing the zeros of the Evans function. For algorithm details, see Appendix A.3.

Multiple solutions We next find numerically an explicit example of two distinct profiles solving the same data. To demonstrate abstract non-uniqueness of profile solutions, our general strategy is to take a piece of the whole-line shock for an unstable wave in the local model, and truncate it to a finite interval. By varying the boundary on the left of this finite interval, we are able to observe a change of sign of the Evans function evaluated at the origin, $D(0)$, indicating non-uniqueness of solutions occurs. Fixing the interval to be $[x_L, x_R] = [-33.17, 2.9]$, we then compute the Evans function at the origin for profiles with varying c_1 and c_2 to find regions in c_1 and c_2 for which $D(0)$ has opposite sign; see Figure 7.1(a)-(b). Explicit parameter pairs $(\hat{c}_1, \hat{c}_2)$ and $(\tilde{c}_1, \tilde{c}_2)$ that correspond to two distinct profiles solving the same data must lie in regions for which $D(0)$ has opposite sign. We note that the nullclines of $D(0)$ shown in Figure 7.1 are nearly parallel, which is expected since these profiles are nearly translationally invariant. Indeed, it is the small eigenvalue corresponding to translational invariance of the whole line profile that makes these computations delicate.

A nice way to find two parameter pairs corresponding to two distinct profiles solving the same data is to look at nullclines of the mappings $M_1(c_1, c_2) := u_L(c_1, c_2) - u_L^*(c_1^*, c_2^*)$ and $M_2(c_1, c_2) := T_L(c_1, c_2) - T_L^*(c_1^*, c_2^*)$. Here (c_1^*, c_2^*) are fixed constants of integration that correspond to the whole line shock, which constants of integration we find by solving for them in the Rankine-Hugoniot equation.

The other terms used in defining M_1 and M_2, that is $u_L(c_1, c_2)$ and $T_L(c_1, c_2)$, are the components of the profiles evaluated at $x = x_L$. We note that these profiles have the same data at $x = x_R$ as the the profile corresponding to (c_1^*, c_2^*). In particular, $u_R(c_1, c_2) = u_R(c_1^*, c_2^*)$ and $T_R(c_1, c_2) = T_R(c_1^*, c_2^*)$. The levels sets of M_1 and M_2 intersect in two locations, which we name $(\hat{c}_1, \hat{c}_2)$ and $(\tilde{c}_1, \tilde{c}_2)$, along the same curves indicating that these constants of integration correspond to two distinct profiles solving the same data; see Figure 7.1 (c)-(d). We plot the profiles corresponding to $(\hat{c}_1, \hat{c}_2)$ and $(\tilde{c}_1, \tilde{c}_2)$ in Figures 7.2(a)-(b). We note that there is approximately a 20% difference between the upper and lower curves over the interval $[-3, 3]$ depicted, in terms of the ratio of the ≈ 0.2 maximum difference between the two curves to the ≈ 1.0 total variation of each curve, far more than can be attributed to numerical error.

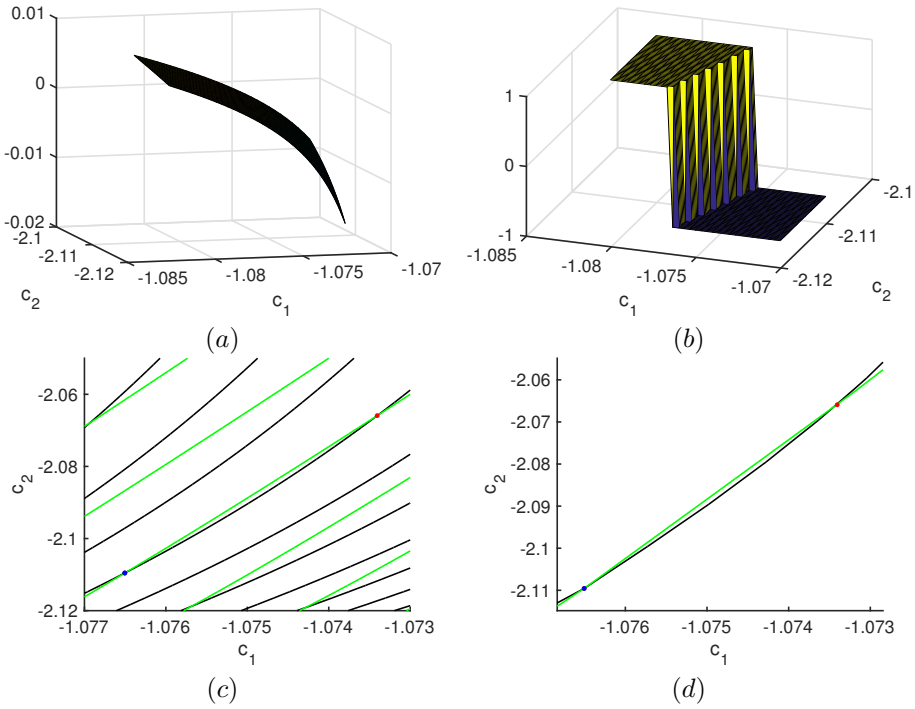

FIGURE 7.1. Figures (a)-(b) demonstrate that $D(0)$ changes sign as c_1 and c_2 vary. Figures (c)-(d) indicate that there are distinct profiles that solve the same data since there are nullclines of M_1 and M_2 that intersect twice. (a) Plot of $D(0)$ against c_1 and c_2. (b) Plot of sign$(D(0))$ against c_1 and c_2. (c) Plot of the nullclines of M_1 and M_2. Dots indicate intersections of the nullclines. (d) Plot of only the two intersecting nullclines seen in (c).

7.2. **Hopf bifurcation.** Using the same shock parameters in the local model that we used to show a bifurcation implying non-uniqueness, but with different choices of left and right boundary, we can show also the existence of a Hopf-bifurcation.

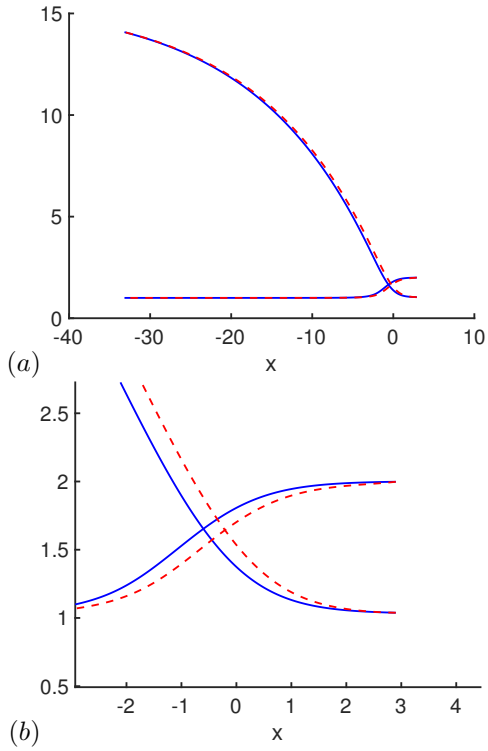

FIGURE 7.2. (a) Plot of the two profiles, solving the same data, against x. The solid blue curves and dashed red curves correspond to the profiles with c_1 and c_2 values plotted as dots with the same colors in Figure 7.1(c)-(d). (b) Zoomed-in picture of (a) near $x = x_R$.

When the finite boundaries are $x_L = -4.3$, $x_R = 4.3$, and the whole-line shock is truncated to $[x_L, x_R]$, the Evans function evaluated on the real line segment $[0, 10^{-3}]$ has no zeros, whereas the image of the Evans function evaluated along $\partial(\{z \in B(0, 1e-3) : \Re(z) \geqslant 0\})$ has winding number of two. Thus, there is a complex conjugate pair of eigenvalues with non-zero imaginary part, indicating that a Hopf-bifurcation occurs; see Figure 7.3 (d)-(e).

APPENDIX A. DOCUMENTATION OF STABLAB

In this appendix, we describe additional computational details geared toward the reader interested in reproducing results. In particular, we provide some references regarding the MATLAB-based package STABLAB that we used extensively throughout this paper. STABLAB [9] is a well-tested package for studying stability of traveling waves using the Evans function. This package has been successfully used in a variety of studies; for example see [14, 6, 4, 11, 12, 21, 31, 19]. For an overview of the methods used in STABLAB, please see [2, 4].

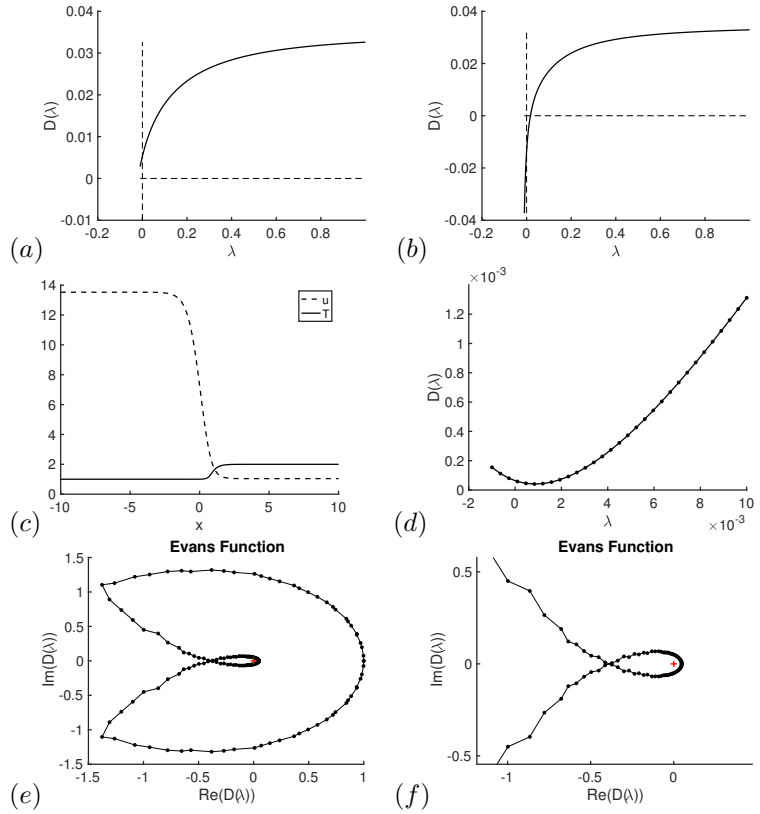

FIGURE 7.3. The parameters of the local model in this figure are $\mu = 0.5$, $\kappa = 1$, $T_- \approx 1.001$, $T_+ = 2$, $\rho_- \approx 0.0769$, $\rho_+ = 1$, $u_+ \approx 1.041$, $u_- \approx 13.53$, and $M \approx 1.041$. (a) Plot of $D(\lambda)$ against λ where $x_L = -0.5$ and $x_R = 2.15$. (b) Plot of $D(\lambda)$ against λ where $x_L = -0.7$ and $x_R = 3.01$. (c) Plot of the whole-line viscous shock profile. (d) Plot of $D(\lambda)$ against λ where $x_L = -4.3$ and $x_R = 4.3$. (e) Plot of $\Im(D(\lambda))$ against $\Re(D(\lambda))$ where $x_L = -4.3$, $x_R = 4.3$, and $D(\cdot)$ is evaluated on $\partial(\{z \in B(0, 1e{-}3) : \Re(z) \geqslant 0\})$. (f) Zoomed-in view of (e).

A.1. **Details of feasibility study.** To verify the correctness of our code when computing the feasibility set, we independently coded by hand a constant step-size Runge-Kutta-Fehlberg four to fifth order scheme and compared it to the solution we obtained using standard suite software in MATLAB. For improved accuracy, for the large scale study we use MATLAB's *ode15s* [38] routine which is an adaptive step, stiff ODE solver. The solver warnings alert us to finite blowup, and testing the sign of a solution tells us whether or not u and e remain positive throughout the unit interval. In Figure 6.1, we plot some examples of the feasible set. Note that the feasible set is unbounded (see Lemma 3.3).

A.2. **Details of the Evans function computations.** We now provide details about numerical conditioning and algorithm choices for the Evans function computations. For background regarding the methods mentioned, please see [4]. To compute the Evans function, we use the the flux coordinates described in Section 3.1 of [7], which is equivalent to computing with coordinates (ρ, u, e, u', e') as described in Section 5. These coordinates are important to use in practice in order to reduce the variation in the image of the Evans function. To improve numerical conditioning of the computation, we evaluate the Evans function wronskian at $x = 1/2$ with ODE solutions given in the definition of the Evans function initialized at $x = 0$ with $\{(0,1,0,0,0)^T, (0,0,1,0,0)^T\}$ and at $x = 1$ with $\{(1,0,0,0,0)^T, (0,1,0,0,0)^T, (0,0,1,0,0)\}$ to recover, as given by Abel's Theorem, a non-vanishing multiple of the Evans function. We also use the method of continuous orthogonalization [25] without the radial equation using Drury's method [18] in order to compute the ODE solution, which resolves computational challenges due to differing growth modes. To verify the correctness of our code, we compute $D(0)$ with the radial equation by initializing the ODE solutions at $x = 0$ only and evolving them to take the determinant at $x = 1$ with the initializing basis there, and check that this matches the value of $D(0)$ computed with the definition given in (5.4).

A.3. **Details of the non-uniqueness study.** The boundary value solver we refer to in Section 7.1 is MATLAB's routine bvp5c, which uses a four-stage Lobatto IIIa formula [27]. We set the tolerance in bvp5c to 1e-6. For the Evans function computations, we use MATLAB's ode15s with the requested relative and absolute error tolerance set to 1e-10 and 1e-12 respectively. The ode15s routine is a variable-step solver based on variable differentiation formulas of first through fifth orders [38].

A.4. **Computational effort.** Computations were done on a desktop with 128GB Ram and a 4.0GHz i7-6950X Intel processor with 25 MB Cache and 10 cores with 20 threads. Computations were done in Matlab using parallel processing. It took 1.37 days of computation to create the data for the final feasibility study figure, Figure 6.1. It took 83.8 days of computation on all 10 cores to compute the data for the final Evans function figure, Figure 6.3. Cumulative computations took longer, exceeding five months. Each of the computations in Section 7 took a substantial part of a day to compute. One of the main reasons the computations were time consuming is stiffness of the associated ODE systems. For instance, for the ounterexample of Section 7, continuation of the profile was necessary in order to achieve required accuracy, simple shooting being prohibitively ill-conditioned. Indeed, this project is similar numerically in scope and delicacy to those described in [3] and [13], which together represent a new level of computational challenge in numerical Evans function studies.

References

[1] J. Alexander, R. Gardner, and C. Jones. A topological invariant arising in the stability analysis of travelling waves. *J. Reine Angew. Math.*, 410:167–212, 1990.
[2] B. Barker. Evans function computation. Master's thesis, Brigham Young University, 2009.
[3] B. Barker, H. Freistühler, and K. Zumbrun. Convex entropy, Hopf bifurcation, and viscous and inviscid shock stability. *Arch. Ration. Mech. Anal.*, 217(1):309–372, 2015.

[4] B. Barker, J. Humpherys, G. Lyng, and J. Lytle. Evans function computation for the stability of travelling waves. *Philosophical Transactions of the Royal Society A: Mathematical, Physical and Engineering Sciences*, 376(2117):20170184, March 2018.
[5] B. Barker, J. Humpherys, G. Lyng, and K. Zumbrun. Viscous hyperstabilization of detonation waves in one space dimension. *SIAM J. Appl. Math.*, 75(3):885–906, 2015.
[6] B. Barker, J. Humpherys, G. Lyng, and K. Zumbrun. Viscous hyperstabilization of detonation waves in one space dimension. *SIAM J. Appl. Math.*, 75(3):885–906, 2015.
[7] B. Barker, J. Humpherys, G. Lyng, and K. Zumbrun. Balanced flux formulations for multidimensional Evans-function computations for viscous shocks. *Quart. Appl. Math.*, 76(3):531–545, 2018.
[8] B. Barker, J. Humpherys, G. Lyng, and K. Zumbrun. Euler versus Lagrange: the role of coordinates in practical Evans-function computations. *SIAM J. Appl. Dyn. Syst.*, 17(2):1766–1785, 2018.
[9] B. Barker, J. Humpherys, J. Lytle, and K. Zumbrun. A MATLAB-based numerical library for evans function computation. *https://github.com/nonlinear-waves/stablab.git*, 2015.
[10] B. Barker, J. Humpherys, and K. Zumbrun. One-dimensional stability of parallel shock layers in isentropic magnetohydrodynamics. *J. Differential Equations*, 249(9):2175–2213, 2010.
[11] B. Barker, M. Johnson, P. Noble, M. Rodrigues, and K. Zumbrun. Stability of viscous St. Venant roll waves: from onset to infinite Froude number limit. *J. Nonlinear Sci.*, 27(1):285–342, 2017.
[12] B. Barker, M. Lewicka, and K. Zumbrun. Existence and stability of viscoelastic shock profiles. *Arch. Ration. Mech. Anal.*, 200(2):491–532, 2011.
[13] B. Barker, R. Monteiro, and K. Zumbrun. Transverse bifurcation of viscous slow MHD shocks. *Physica D: Nonlinear Phenomena*, 420:132857, June 2021.
[14] B. N. Barker. Stability of MHD shock waves. Master's thesis, Brigham Young University, 2020.
[15] G. K. Batchelor. *An introduction to fluid dynamics*. Cambridge Mathematical Library. Cambridge University Press, Cambridge, paperback edition, 1999.
[16] L. E. J. Brouwer. Über Abbildung von Mannigfaltigkeiten. *Mathematische Annalen*, 71(1):97–115, March 1911.
[17] G. Dinca and J. Mawhin. *Brouwer degree, the Core of Nonlinear Analysis*, volume 95 of *Progress in Nonlinear Differential Equations and Their Applications*. Birkhäuser Basel, 2021.
[18] L. Drury. Numerical solution of Orr-Sommerfeld-type equations. *J. Comput. Phys.*, 37(1):133–139, 1980.
[19] Ozbag F. and S. Schecter. Stability of combustion waves in a simplified gas–solid combustion model in porous media. *Philosophical Transactions of the Royal Society A: Mathematical, Physical and Engineering Sciences*, 376(2117):20170185, March 2018.
[20] R. A. Gardner and K. Zumbrun. The gap lemma and geometric criteria for instability of viscous shock profiles. *Comm. Pure Appl. Math.*, 51(7):797–855, 1998.
[21] A. Ghazaryan, S. Lafortune, and V. Manukian. Spectral analysis of fronts in a Marangoni-driven thin liquid film flow down a slope. *SIAM Journal on Applied Mathematics*, 80(1):95–118, January 2020.
[22] M. W. Hirsch. *Differential topology*, volume 33 of *Graduate Texts in Mathematics*. Springer-Verlag, New York, 1994. Corrected reprint of the 1976 original.
[23] J. Humpherys, G. Lyng, and K. Zumbrun. Spectral stability of ideal-gas shock layers. *Arch. Ration. Mech. Anal.*, 194(3):1029–1079, 2009.
[24] J. Humpherys, G. Lyng, and K. Zumbrun. Multidimensional stability of large-amplitude Navier-Stokes shocks. *Arch. Ration. Mech. Anal.*, 226(3):923–973, 2017.
[25] J. Humpherys and K. Zumbrun. An efficient shooting algorithm for Evans function calculations in large systems. *Phys. D*, 220(2):116–126, 2006.
[26] D. Kawashima and Y. Shizuta. On the normal form of the symmetric hyperbolic-parabolic systems associated with the conservation laws. *Tohoku Math. J. (2)*, 40(3):449–464, 1988.
[27] J. A. Kierzenka and L. F. Shampine. A bvp solver that controls residual and error. *JNAIAM J. Numer. Anal. Ind. Appl. Math*, pages 1–2, 2008.
[28] J. R. Kweon and R. B. Kellogg. Compressible Navier-Stokes equations in a bounded domain with inflow boundary condition. *SIAM J. Math. Anal.*, 28(1):94–108, 1997.

[29] P. D. Lax. *Hyperbolic systems of conservation laws and the mathematical theory of shock waves*. Society for Industrial and Applied Mathematics, Philadelphia, Pa., 1973. Conference Board of the Mathematical Sciences Regional Conference Series in Applied Mathematics, No. 11.

[30] P.-L. Lions. *Mathematical topics in fluid mechanics. Vol. 2*, volume 10 of *Oxford Lecture Series in Mathematics and its Applications*. The Clarendon Press, Oxford University Press, New York, 1998. Compressible models, Oxford Science Publications.

[31] J. Lytle. *Stability of Planar Detonations in the Reactive Navier-Stokes Equations*. PhD thesis, Brigham Young University, 2017.

[32] B. Melinand and K. Zumbrun. Existence and stability of steady compressible Navier-Stokes solutions on a finite interval with noncharacteristic boundary conditions. *Physica D: Nonlinear Phenomena*, 394:16 – 25, 2019.

[33] B. Melinand and Z. Zumbrun. Existence and behavior of steady solutions on an interval for general hyperbolic-parabolic systems of conservation laws. *Arxiv: 2112.03995*, 2021.

[34] J.W. Milnor. *Topology from the differentiable viewpoint*. The University Press of Virginia, Charlottesville, Va., 1965. Based on notes by David W. Weaver.

[35] V. V. Prasolov. *Elements of combinatorial and differential topology*, volume 74 of *Graduate Studies in Mathematics*. American Mathematical Society, Providence, RI, 2006. Translated from the 2004 Russian original by Olga Sipacheva.

[36] F. Rousset. Inviscid boundary conditions and stability of viscous boundary layers. *Asymptot. Anal.*, 26(3-4):285–306, 2001.

[37] D. Serre and K. Zumbrun. Boundary layer stability in real vanishing viscosity limit. *Comm. Math. Phys.*, 221(2):267–292, 2001.

[38] L.F. Shampine and M.W. Reichelt. The MATLAB ODE suite. *SIAM Journal on Scientific Computing*, 18(1):1–22, January 1997.

[39] B. Texier and K. Zumbrun. Transition to longitudinal instability of detonation waves is generically associated with Hopf bifurcation to time-periodic galloping solutions. *Comm. Math. Phys.*, 302(1):1–51, 2011.

[40] K. Zumbrun. Multidimensional stability of planar viscous shock waves. In *Advances in the theory of shock waves*, volume 47 of *Progr. Nonlinear Differential Equations Appl.*, pages 307–516. Birkhäuser Boston, Boston, MA, 2001.

[41] K. Zumbrun. Stability of noncharacteristic boundary layers in the standing-shock limit. *Trans. Amer. Math. Soc.*, 362(12):6397–6424, 2010.

[42] K. Zumbrun and P. Howard. Errata to: "Pointwise semigroup methods, and stability of viscous shock waves" [Indiana Univ. Math. J. (47) (1998), no. 3, 741–871; MR1665788 (99m:35157)]. *Indiana Univ. Math. J.*, 51(4):1017–1021, 2002.

[43] K. Zumbrun and D. Serre. Viscous and inviscid stability of multidimensional planar shock fronts. *Indiana Univ. Math. J.*, 48(3):937–992, 1999.

Manuscript received October 26, 2021,
revised September 8, 2022,
accepted December 31, 2023.

Blake BARKER
Brigham Young University, Provo, UT 84602. Research partially supported under NSF grant no. DMS-140087
blake@mathematics.byu.edu

Benjamin MELINAND
CEREMADE, CNRS, Université Paris-Dauphine, Université PSL, 75016 PARIS, FRANCE
melinand@ceremade.dauphine.fr

Kevin ZUMBRUN
Indiana University, Bloomington, IN 47405. Research of K.Z. was partially supported under NSF grant no. DMS-1700279.
kzumbrun@indiana.edu